ACS APPLIED MATERIALS & INTERFACES

www.acsami.org Research Article

Stack Thermo-Osmotic System for Low-Grade Thermal Energy Conversion

Ji Li,[‡] Zikang Zhang,[‡] Runze Zhao, Bo Zhang, Yunmin Liang, Rui Long, Wei Liu, and Zhichun Liu*

Cite This: *ACS Appl. Mater. Interfaces* 2021, 13, 21371−21378 Read Online

ACCESS | Metrics & More | Article Recommendations | Supporting Information

ABSTRACT: Thermo-osmotic energy conversion (TOEC) technology, developed from membrane distillation, is an emerging method that has the potential of obtaining electricity efficiently from a low-grade heat source but faces the difficult problem of pump power loss. In this study, we build a novel TOEC system with a multistage architecture that can work without pump assistance. The experiment system, made of cheap commercial materials, can obtain a power density of 1.39 ± 0.25 W/m^2, with a heating temperature of 80 °C, and its efficiency increased linearly with the total stage number. A theory calculation shows that a 30-stage system with a specific membrane and a working pressure of 5.0 MPa can obtain an efficiency of 2.72% with a power density of 14.0 W/m^2. By a molecular dynamics simulation, it is shown that a high-performance membrane has the potential to work at 40 MPa. This study proves that TOEC technology is a practical and competitive approach to covert low-grade thermal energy into power efficiently.

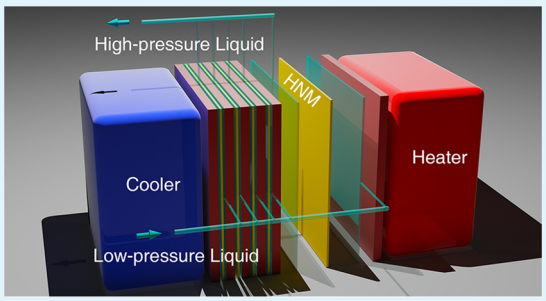

KEYWORDS: *thermo-osmosis, renewable energy, waste heat, pressure-retarded membrane distillation, hydrophobic nanoporous membranes, nanofibers*

Downloaded via HUAZHONG UNIV SCIENCE & TECHNOLOGY on May 31, 2021 at 12:18:38 (UTC).
See https://pubs.acs.org/sharingguidelines for options on how to legitimately share published articles.

1. INTRODUCTION

The global energy consumption still mainly relies on fossil fuels, a practice that is polluting and unsustainable. Low-grade thermal energy (below 80 °C) is widely distributed in solar, geothermal, and industrial activities.[1,2] So, it is very urgent and valuable to develop clean, cheap, efficient, convenient, and practical methods to convert low-grade heat into power.[3−6] Thermo-osmosis is a mass-transfer phenomenon across a membrane, driven by a transmembrane temperature difference, and proceeding with an enthalpy change of working media.[7−9] Thermo-osmotic energy conversion (TOEC) is a newly developed heat conversion method based on the thermo-osmosis process across a hydrophobic nanoporous membrane.[10−12] TOEC has advantages including efficient, cheap, clean, easy to scale, and compatible with low-temperature sources.[13] TOEC was developed from the traditional membrane distillation devices, and it obtains power from the hydraulic pressure energy of the condensation liquid, so it is also called pressure-retarded membrane distillation.[14,15] By a theory calculation, a TOEC system with an ideal heat regenerator can have an attractive efficiency of 4.1% for a 60 °C heat source, which is equivalent to 34% of the Carnot efficiency.[13]

As shown in Figure 1a, if a temperature gradient is added across a hydrophobic porous membrane, the mass can be transferred from the hot liquid pool to the cold liquid pool with overcoming the transmembrane hydraulic pressure increment, ΔP. And a TOEC system utilizes the mass flux and the pressure increment to generate power. If water is employed as the working media, by Antoine and Kelvin equations, it is estimated that a transmembrane temperature difference of 1 °C has the potential to generate a hydraulic pressure increment of 6−7 MPa on the condensation side, which is greater than the osmotic pressure of seawater. And the potential pressure increment P_{TO} can also be estimated by[13]

$$P_{TO} = \frac{q_M}{V_M}\left(1 - \frac{T_2}{T_1}\right) \quad (1)$$

where q_M is the molar vaporization enthalpy of the working media, V_M is the molar volume of the working liquid, and T_1 and T_2 are the surface temperatures of the membrane. Like pressure-retarded osmosis,[16] the power density of a TOEC system can be estimated by $w = V_w \cdot P_w$, where V_w is the volume flux of the condensation liquid, and P_w is the working pressure or the transmembrane hydraulic pressure increment in operation. A high-performance TOEC system should utilize the potential pressure increment efficiently; that is, the working pressure should be closed to the potential pressure increment,

Received: February 21, 2021
Accepted: April 19, 2021
Published: April 27, 2021

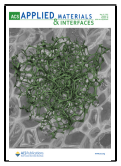

© 2021 American Chemical Society

https://doi.org/10.1021/acsami.1c03395
ACS Appl. Mater. Interfaces 2021, 13, 21371−21378

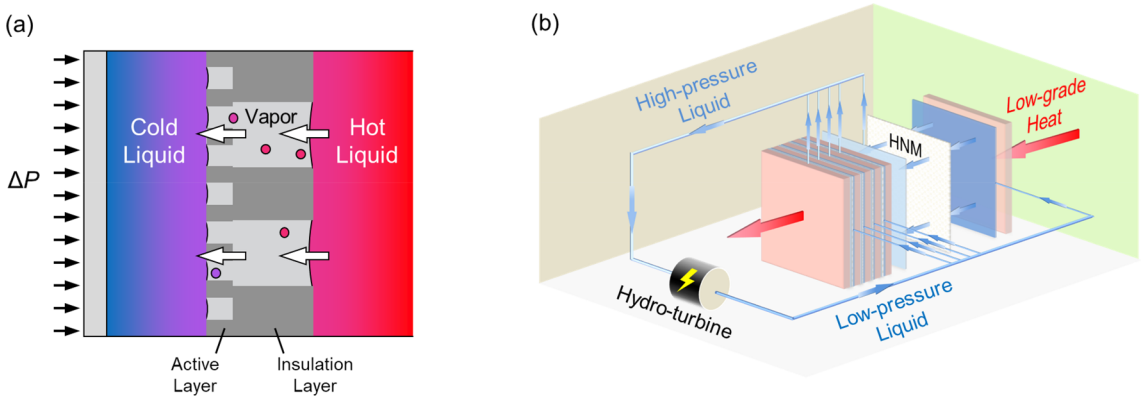

Figure 1. (a) Schematic diagram of a TOEC process across a hydrophobic membrane. If adding a transmembrane temperature gradient, by the mass driving force of vapor pressure gradient, the working liquid can be transferred from the hot side to the cold side by vaporization, permeation, and condensation. To balance the vapor permeation ability and transmembrane conduction loss, the membrane should have a composite structure. The active layer has a small pore size to repel the high hydraulic pressure on the cold side, while the insulation layer has a large pore size to reduce the permeation resistance and a relatively large thickness to reduce the heat conduction loss. (b) Schematic illustration of the stack thermo-osmotic energy conversion system. Low-pressure liquid flows into the evaporation chamber of a stage, absorbs heat, evaporates, then permeates across the hydrophobic nanoporous membrane (HNM), condenses into the high-pressure liquid, and finally flows out. The hydraulic energy of the outlet liquid can be converted into electricity by a turbine. To improve the energy efficiency, the released heat of a stage can be conducted to the next stage and can then be reused. The flow of the cycle is driven by the pressure gradient, so it does not need a pump to maintain working.

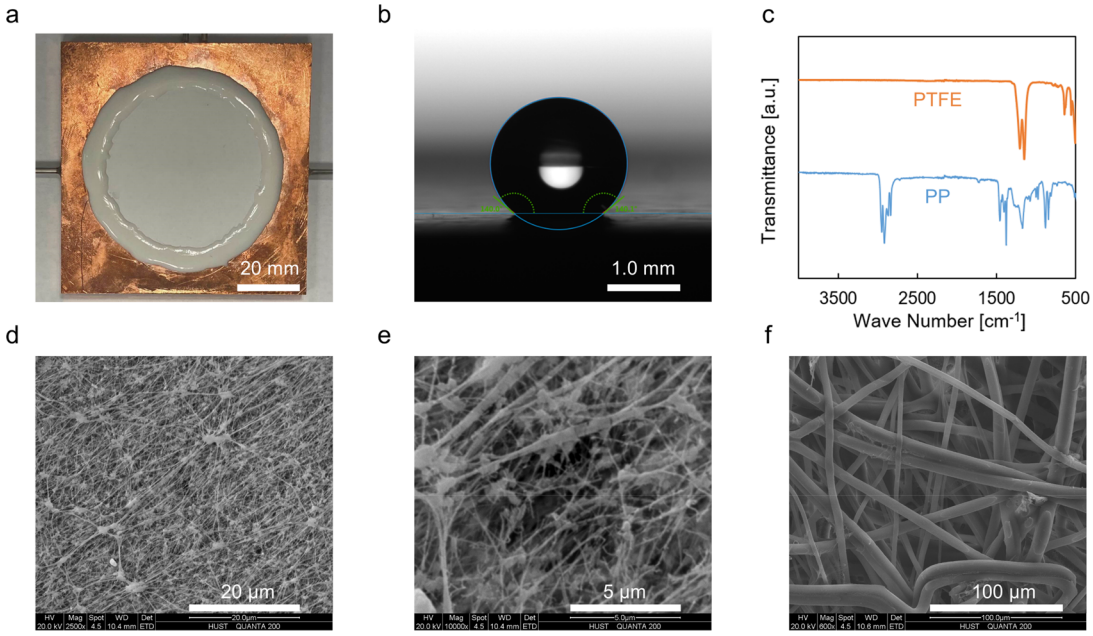

Figure 2. (a) Photograph of a working plate. The membrane is glued on the working plate by silicone rubber, with a working area of ~18 cm^2. (b) The contact angle of a water drop on the hydrophobic membrane surface is 142.0 ± 3.4°. (c) Fourier-transform infrared spectroscopy of the composited membrane. a.u., arbitrary units. The active layer on the two sides is made of PTFE nanofiber, and the insulation layer in the middle is made of PP microfiber. (d, e) Environmental scanning electron microscope images of the active layer. (f) Environmental scanning electron microscope image of the insulation layer.

but it is not easy. For the heating and cooling temperatures of 80 and 40 °C, it can generate a potential pressure increment of 264 MPa, which is very difficult to utilize, mainly because the membrane will be wetted at a high hydraulic pressure, leading to a transmembrane leakage. Considering a membrane with a through pore size of 20 nm and a water contact angle of 120°, it has a maximum working pressure of 6.4 MPa, estimated by the Young−Laplace equation, which is still two orders of magnitude lower than the potential pressure increment for 80 and 40 °C.

A possible solution of utilizing the P_{TO} efficiently is combining a TOEC device with a counter-flow heat exchanger to recover the dissipated heat of the condensation side.[13] This method will reduce the local transmembrane temperature difference, so even a low working pressure can still achieve a high partial efficiency of 4.1%. However, because of its large flow rate, this method faces the difficult problem of a high pump power loss, which significantly reduces the actual efficiency of the system and restricts its application. Besides, another prospect of TOEC technology is embedded in a membrane distillation system to obtain pure water and recover some of the electricity cost, which still needs pump power input.[17,18] In this study, to prove the practicability and competition of the TOEC method for utilizing low-grade heat,

https://doi.org/10.1021/acsami.1c03395
ACS Appl. Mater. Interfaces 2021, 13, 21371−21378

Table 1. Properties of the Membrane Employed in the Experiment and Prediction

	experiment (with double active layers)		prediction (with single active layer)	
	active layer	insulation layer	active layer	insulation layer
nominal pore size, μm	0.1[a]	20[b]	0.020	0.500
porosity	0.854 ± 0.028	0.605 ± 0.014	0.70	0.70
thickness, μm	20 ± 6	242 ± 8	10	300
tortuosity[c]	1.08	1.29	1.20	1.20
$B_{w,i}$, kg/(Pa·s·m^2)	5.35×10^{-6}	4.93×10^{-7}	1.26×10^{-6}	3.65×10^{-7}
$B_{w,c}$, kg/(Pa·s·m^2)	4.09×10^{-7}		2.86×10^{-7}	

[a]Provided by the manufacturer. [b]Estimated by the SEM photograph, which has little influence on the calculation of its vapor permeability coefficient dominated by the diffusion resistance. [c]Estimated by $\tau = \varepsilon^{-0.5}$.[21]

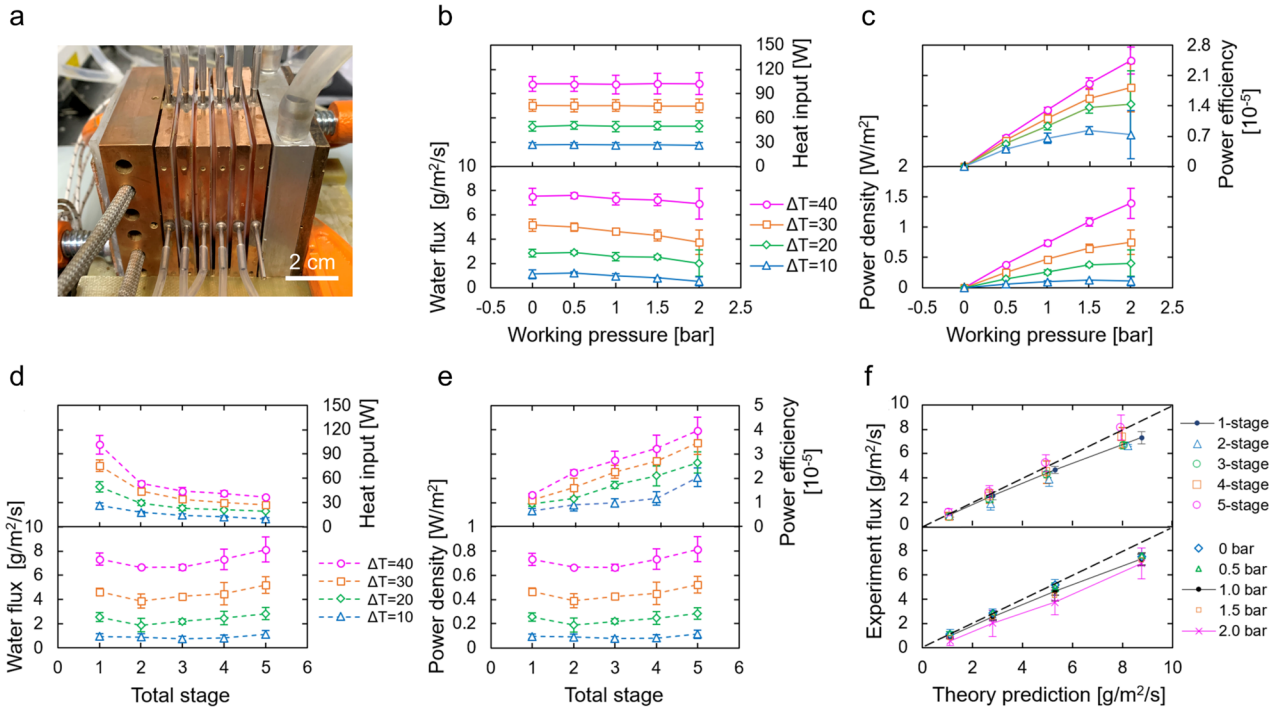

Figure 3. (a) Image of the experiment device with five working stages (six working plates). The working plates were stacked and placed between an electric heater and a water-cooling plate. (b, c) Experiment performances of the single-stage TOEC system with the working pressure. The water and power density are normalized to the working membrane area, and the heat input is the total thermal energy input. (d, e) Experiment performances of the multistage TOEC system with total working stage, while the working pressure was kept at 1.0 bar. The flux, heat input, power density, and efficiency are the total values of all stages. (f) The experiment mass flux with the theory calculation result. Error bar: standard deviation.

we build a novel stackable TOEC system, which can work without a pump assistant and can output net power. And we theoretically predict a stack TOEC system that can achieve a very attractive potential performance if employing a specific membrane.

As shown in Figure 1b, we designed a stack TOEC system to convert thermal energy into power based on the thermo-osmosis effect across a hydrophobic nanoporous membrane. The main subassemblies of the system include working stages, flow pipes, and a hydraulic turbine. Each working stage has two liquid chambers; one is the evaporation chamber, and the other is the condensation chamber. The chambers are separated by working plates and membranes. All the materials can be obtained with a low price.[19] When the cycle works, a low-pressure liquid flows into the evaporation chamber, absorbs heat from the high-temperature heat source or the previous stage, then vaporizes and permeates through the membrane, condenses into the high-pressure liquid in the condensation chamber, and finally flows out the stage and across the water turbine with the pressure energy converted to electricity. The system recycles heat energy through a multistage architecture to improve its total thermal efficiency, and each stage will work at a lower temperature difference, so even a low working pressure can obtain a high efficiency. Besides, the flow circulation is several orders lower than that of traditional TOEC or membrane distillation devices, and the flow can be driven by the thermo-osmosis effect if the noncondensable gas has been removed from the closed cycle.[20]

2. MATERIALS

As shown in Figure 2, a commercial membrane was employed for maintaining the transmembrane pressure difference. The properties of the membrane are presented in Table 1. It has a thickness of 282 ± 9 μm and a water drop contact angle of 142.0 ± 3.4°. The membrane has a composited structure with two active layers on the two surfaces

https://doi.org/10.1021/acsami.1c03395
ACS Appl. Mater. Interfaces 2021, 13, 21371−21378

and an insulation layer in the interlayer. The active layer is made of poly(tetrafluoroethylene) PTFE nanofiber, with a nominal pore size of 0.1 μm to resist the hydraulic pressure. And the insulation layer is made of polypropylene (PP) microfiber with a large pore size to reduce heat conduction loss without increasing too much vapor permeate resistance. The vapor permeability coefficient of the composited membrane, $B_{w,c}$, is estimated as 4.09×10^{-7} kg/(Pa·s·m^2) with air in the membrane pore (Supporting Information, section 2).

3. RESULTS AND DISCUSSION

The working stages were placed between an electric heater and a water-cooling plate (Figure 3a). The experiment was performed in constant temperature and working pressure conditions. The heating temperature was set to 50−80 °C, while the cooling temperature was kept at 40 °C for all conditions so that the heat could be dissipated to the environment by a passive cooling method without consuming power. Figure 3b,c shows the performances including water permeate flux, heat input, power density, and power efficiency of the single-stage system. All the performances increased with the temperature difference due to a larger driven force. It is observed that the water flux might decrease with the working pressure at a temperature condition, which should decrease mainly because of a partial leakage of the membrane under a hydraulic pressure difference. On the basis of the experiments, the leakage condition varied with the membrane, which mainly depends on the large-sized pores of the membrane, since we did not find a porosity difference between the test batch. When the heating temperature was set to 80 °C and the working pressure was 2.0 bar, a high-performance membrane had reached the power density of 1.60 W/m^2, which is close to the following theory prediction, while a low-performance membrane only obtained 1.11 W/m^2. When the heating temperature is 50 °C, some membranes can still work with a pressure higher than 3.5 bar, but some membranes cannot even work with a pressure less than 2.5 bar. Besides, the decrease in water flux with pressure could also be attributable to the membrane compaction. The compaction effect would be much stronger for a membrane with a high porosity, and it could be much slighter for the membrane with a porosity less than ∼70%.[15] The heat input Q_{in} was the heating power of the electric heater, and it changed little with the working pressure, which proved that the heat flux transferred by evaporation did not change a lot. The power efficiency η was calculated by $\eta = W/Q_{in}$, where W is the total power rate. Because of the water flux decrement at the high working pressure, the power density and the efficiency did not always increase with the working pressure.

Figure 3d,e shows the performances of the cases with different total stage numbers. To reduce the influence of leakage on the water flux, the working pressure was kept to 1.0 bar. These performances still increased with heating temperature. An interesting thing is, with the total stage number increase, the water flux did not change a lot, but the heat input reduced quickly, and the power efficiency increased linearly. For the five-stage system, it can achieve a total thermal efficiency of 93.3% at 80 °C, while the local thermal efficiency of a direct contact membrane distillation system with ideal heat insulation property is below 80% for most cases. The input heat from a heating plate would be transferred to the cooling plate or be dissipated to the environment by the other surfaces. With more working stages, the side heat transfer would be stronger due to the larger side area, but the total heat input still decreased, because the heat transfer from the heating plate to the cooling plate was reduced, benefiting from the larger heat transfer resistance. And the water flux did not reduce significantly with the heat input due to the higher efficiency of the total stages. The experiment results also indicate that the performance of the stack TOEC system still has a large potential to improve with more working stages and better membranes.

To estimate the performance and potential of the stack TOEC system, we built a model based on the heat and mass-transfer theory of membrane distillation (Supporting Information, section 2).[15,22] Although the theory is simple, it has widely and successfully described the behavior of membrane distillation and TOEC systems.[23,24] The comparison between the theory model prediction and experiment results is presented in Figure 3f. For the single-stage system, it can predict well when the working pressure is below 1.0 bar, and the experiment flux is a bit lower than the prediction value for a working pressure of 2.0 bar, because the model does not consider leakage. It is surprising that the model without considering heat dissipation loss by stage sides can still predict well the water flux of the multistage system. As shown in Figure 4a, because the total temperature difference of the multistage system was kept, a heat dissipation loss will reduce the temperature difference of the final stage, and it will increase the difference of the initial stage. So, as shown in Figure 4b, the total water flux of an experiment system is not sensitive to the heat dissipation loss and can be predicted well by the theory model. Besides, on the basis of the theory calculation, for the single-stage system with the heating temperature of 80 °C, it is estimated that ∼44.5 W, or 43.6%, of input heat was transferred by the working area, which contributed to the water flux. The rest of the heat was dissipated to the environment or was conducted to the cooling plate by the sealing silicone between stages. For a large-scale system, the dissipation by side surface and the ineffective conduction area

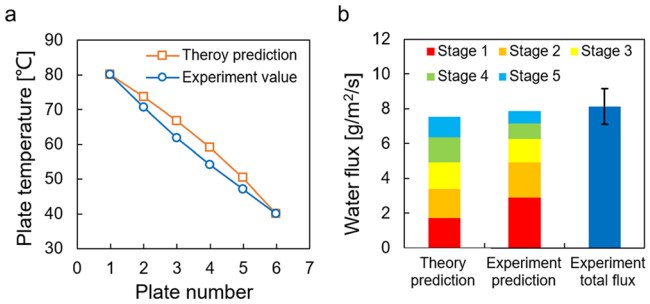

Figure 4. Comparison of the experiment and theory prediction results for a five-stage system. The working pressure was 1.0 bar, and the working temperatures were 80 and 40 °C. (a) Plate temperature distribution with working plate. For the experiment, due to the heat dissipation to the environment, the heat flux and temperature difference across a stage decreased with the plate number. And the plate temperature distribution curve was a little lower than the theory prediction result. (b) Water flux distribution with working stage. The water flux distribution of the experiment was predicted by the plate temperature distribution. Relative to theory prediction, the experiment had higher fluxes in the initial stages and lower fluxes in the final stages. Because the total temperature difference is kept, the total water flux of a real module is not sensitive to the heat dissipation loss. And the total water flux of an experiment system can be described well by the theory model even when the model did not consider the heat dissipation.

https://doi.org/10.1021/acsami.1c03395
ACS Appl. Mater. Interfaces 2021, 13, 21371−21378

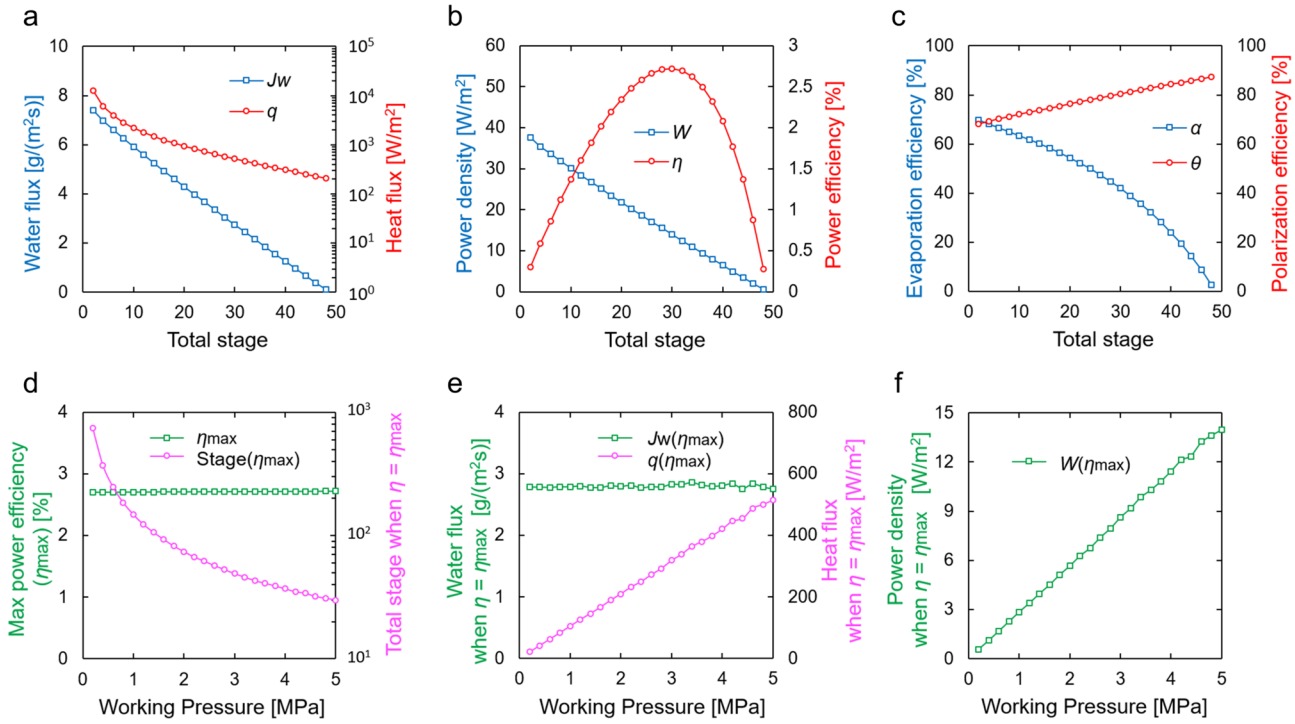

Figure 5. Theory performances of a stack TOEC system with heat source temperatures of 80 and 40 °C. (a−c) Performances with the total working stage number while the working pressure is kept at 5.0 MPa. (d) The maximum power efficiency and the suitable working stage number with the working pressure. (e, f) Performances with the working pressure when the working stage number is set for the maximum power efficiency.

between stages can be much reduced. Considering the proportion of the effective heat, as shown in Figure 3b, the mass flux reduction at a high pressure is more likely to result from leakage rather than membrane compression, since the heat input did not change a lot with working pressure.

For a TOEC system, only the heat transfer induced by a phase change across the membrane can generate power. The evaporation efficiency α is defined by $\alpha = J_w \cdot H_{vap}/q/n$, where H_{vap} is the vaporization enthalpy of the working media, and n is the total stage number. A large pore size and low air partial pressure in the pores benefit the evaporation efficiency. The polarization efficiency θ is defined by

$$\theta = \frac{\sum_{i=1}^{n} (T_{1,i} - T_{2,i})}{T_h - T_c} \quad (2)$$

where $T_{1,i}$ and $T_{2,i}$ are membrane surface temperatures of a stage, and T_h and T_c are heating and cooling temperatures. A large membrane thickness and low heat resistance of other solid and liquid layers benefit the polarization efficiency. On the basis of the theory calculation, with the source temperatures of 80 and 40 °C and a working pressure of 1.0 bar, the one-stage and five-stage experiment systems have high evaporation efficiencies of 74.8% and 71.9% and comparatively high temperature polarization efficiencies of 54.1% and 56.7% (higher than most membrane distillation cases), which proves that the parameters of the experiment system had been chosen well.

On the basis of the model, we also predicted the performances of a multistage TOEC system employing a high-performance membrane with a nominal pore size of 20 nm, a porosity of 70%, and a thickness of 310 μm, and it can work well at a hydraulic pressure of 5.0 MPa. Figure 5a−c shows the theory performances of the system with heating and cooling temperatures of 80 and 40 °C, a working pressure of 5.0 MPa, and different total stage numbers. The performances include mass flux, heat flux, power density, power efficiency, evaporation efficiency, and polarization efficiency. With the increase of the total stage number, the heat flux of the system decreases exponentially, leading to the increment of the power efficiency. However, as described by the Kelvin equation, because of the vapor pressure difference loss, the water flux and power density also decrease linearly with the total stage, and the efficiency will not increase without limit. When the total stage number is 30, the power efficiency reaches the maximum of 2.72%, which is 24.0% of the Carnot limit, with a power density of 14.0 W/m^2, a heat flux of 514.3 W/m^2, an evaporation efficiency of 42.0%, and a polarization efficiency of 80.3%. If combining the system with a photovoltaic panel, a 22-stage system can obtain a power density of 20.3 W/m^2 with a heating temperature of 80 °C and a heat flux of 817.6 W/m^2. And if the air in the cycle and membrane pores is degassed, it predicts that the 32-stage system can obtain a maximum efficiency of 3.86% with a power density of 23.1 W/m^2 (Supporting Information, Figure 5). These good results prove the competition of the stack TOEC technology, which still has a greater potential to improve by optimizing the membrane parameters. However, note that this prediction did not consider leakage or membrane compression, and an actual system should employ a high-hydraulic-pressure-repellent membrane to obtain the predicted performance.

As Straub et al. discussed before,[13] TOEC technology could have a much higher potential efficiency relative to other low-grade heat conversion methods. However, it should combine with a turbine to convert hydraulic energy to electricity, which restricts its application as a small and portable electricity source before nanoturbine technology has been developed and reached maturity. Besides, like pumped hydro energy storage

https://doi.org/10.1021/acsami.1c03395
ACS Appl. Mater. Interfaces 2021, 13, 21371−21378

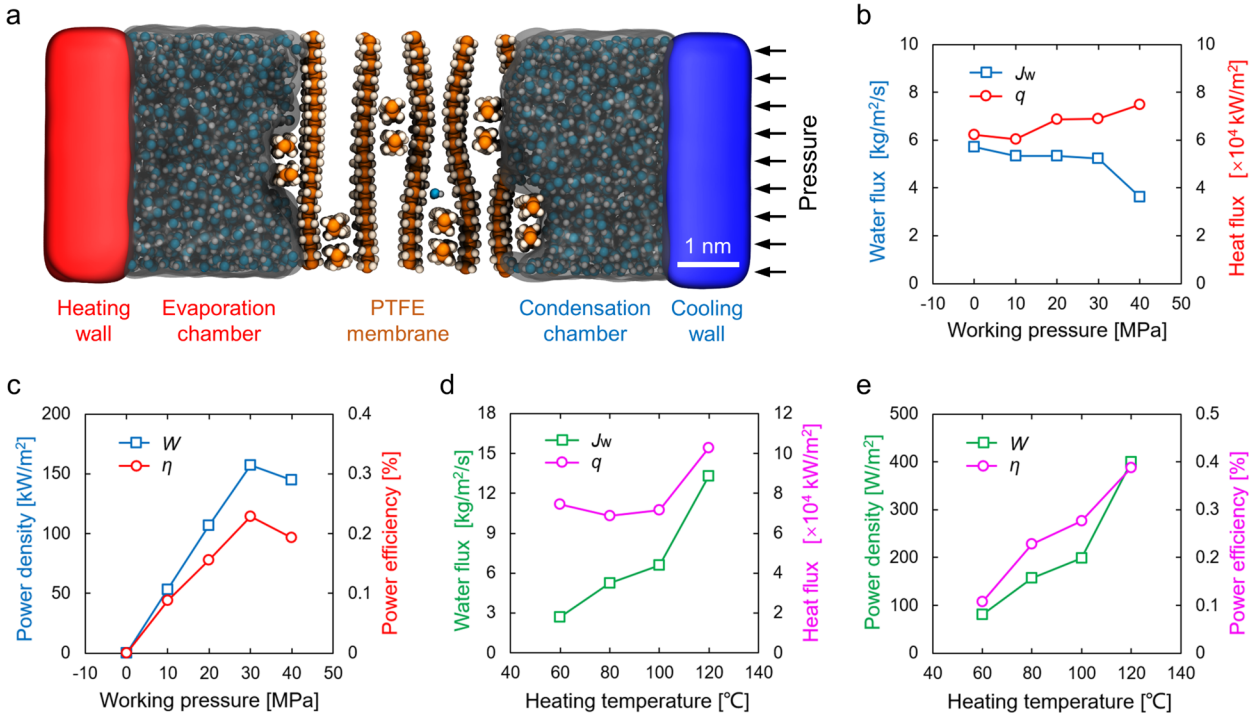

Figure 6. Molecular dynamics simulation for a nanoscale single-stage TOEC system. (a) Illustration of the simulation system. A nanofiber PTFE membrane with a pore size of 3.0 nm and a thickness of ∼5.5 nm was set between two liquid chambers. The temperatures of the liquids were controlled by two copper pistons. (b, c) Performances of the nanoscale TOEC system with the working pressure, while the heating and cooling temperatures were 80 and 60 °C. The nanofiber PTFE membrane can resist a hydraulic pressure difference of 40 MPa, and it will be wetted at 50 MPa. (d, e) Performances of the nanoscale TOEC system with the heating temperature, while the temperature difference is kept at 20 °C and the working pressure is kept at 30 MPa.

technology, another solution for a small-sized system is employing a water reservoir at a high place, and it can convert the gravitational potential energy of water head to electricity by a turbine intermittently. Furthermore, also note that, if not degassing the air in the TOEC system, the working stage should be placed vertically or slantwise to prevent non-condensable gas from impeding the liquid supply.

As shown in Figure 5d, it is theoretically predicted that, if the working pressure is not very high, the system can still reach a same-high efficiency. But it needs many more working stages, which reduces the fluxes due to the larger resistances of heat and mass transfer (Figure 5e,f). So, a high working pressure is essential for a stack TOEC system, which can improve the power density and reduce the investment of the working plates. A previous experimental study has proved that a working pressure of 2.7 MPa is achievable;[12,25] however, the performance decreased more quickly than theory limitation mainly due to membrane compression. So, the question is can a high-performance membrane resist a superhigh pressure and still work well?

As shown in Figure 6, by a molecular dynamics simulation, we proved that a TOEC system employing a PTFE nanofiber with a pore size of ∼3.0 nm can work with a huge working pressure of 40 MPa, and it can keep the pore structure and the vapor permeation. This result indicates that fabricating a high-hydraulic-pressure-repellent membrane is possible.[26,27] And because of the very low transfer resistances of the nanoscale system, it can obtain superhigh power densities, 80.4 kW/m^2 for the heating temperature of 60 °C and 400 kW/m^2 for 120 °C, with a temperature difference of 20 °C.[28−30] However, because of the low stage number, low evaporation efficiency, and low polarization efficiency, the power efficiency of the simulation system is less than 0.39%. So, as described before, a high-hydraulic-pressure-repellent membrane with a small pore size should be combined with an insulation layer with enough thickness and a large pore size to improve the polarization efficiency without increasing too much vapor resistance. Restricted by calculation resources, we cannot simulate the TOEC process of the PTFE nanofiber membrane with a micrometer-thick insulation layer, but it can still be confidently predicted that the composted membrane will perform very well.

4. CONCLUSIONS

In this study, to prove the feasibility and competition of thermo-osmosis energy conversion technology for a low-grade heat conversion, we developed a novel stackable TOEC system with a multistage architecture, and it can work without pump power loss. The experiment system, made of cheap commercial materials, can output a power density of 1.39 ± 0.25 W/m^2, with a working pressure of 2.0 bar, a heating temperature of 80 °C, and a cooling temperature of 40 °C. More importantly, the efficiency of the system increased linearly with the total stage number. Theory calculation shows that a 30-stage TOEC system with a specific membrane and a working pressure of 5.0 MPa can obtain an efficiency of 2.72% with a power density of 14.0 W/m^2 for the temperatures of 80 and 40 °C. By a molecular dynamics simulation, a working pressure of 40 MPa was achieved for a nanofiber membrane, which shows the promising prospect of a high-performance TOEC system.

https://doi.org/10.1021/acsami.1c03395
ACS Appl. Mater. Interfaces 2021, 13, 21371−21378

5. METHODS

The working plate is made of copper with a thickness of 0.75 cm, and the PTFE membrane was glued on the plate by silicone rubber with an effective area of ∼18 cm^2. The working stages were stacked and placed between a heating plate and a cooling plate. A needle valve was employed to regulate the pressure of outlet liquid.[15,17] The detailed setup of the lab-scale system is illustrated in Supporting Information, Figure 1.

A theory calculation model for the stacked TOEC system was built based on the previous works of membrane distillation and thermo-osmosis.[13−15,17,22] To simplify the calculation, several reasonable assumptions were made: (a) ignoring the heat transferred by the unworked area and ignoring the heat exchange between the system and the environment; (b) ignoring the membrane compression; (c) the maximum pore size of the membrane is small enough to repel the working pressure, and the transmembrane liquid leakage is neglected; and (d) the physical properties are unchanged for the calculated condition.[15] With these assumptions, the problem is similar to a membrane distillation case, while the local vapor pressure decrement of the condensation side should be considered under a hydraulic pressure. The model and calculation details are described in Supporting Information, section 2.

The molecular dynamics simulations were performed by the package LAMMPS and were visualized by VMD.[31,32] The size of the simulation domain is 3.97 × 3.97 × 14.5 nm^3, and periodic boundary conditions were set to directions x and y. The potentials of water, PTFE molecules, and copper atoms were TIP3P,[33] OPLS-AA,[34] and 12−6 Lennard-Jones.[35] Each simulation condition was integrated for 40.0 ns in the NVE process, with a time step of 1.0 fs.[36,37] More simulation details are presented in the Supporting Information, section 3.

■ ASSOCIATED CONTENT

Supporting Information

The Supporting Information is available free of charge at https://pubs.acs.org/doi/10.1021/acsami.1c03395.

Experiment details; theory calculation details; molecular dynamics simulation details; supplementary data (PDF)

■ AUTHOR INFORMATION

Corresponding Author

Zhichun Liu − *School of Energy and Power Engineering, Huazhong University of Science and Technology, Wuhan 430074, China;* orcid.org/0000-0001-9645-3052; Email: zcliu@hust.edu.cn

Authors

Ji Li − *School of Energy and Power Engineering, Huazhong University of Science and Technology, Wuhan 430074, China*

Zikang Zhang − *School of Energy and Power Engineering, Huazhong University of Science and Technology, Wuhan 430074, China*

Runze Zhao − *School of Energy and Power Engineering, Huazhong University of Science and Technology, Wuhan 430074, China*

Bo Zhang − *School of Energy and Power Engineering, Huazhong University of Science and Technology, Wuhan 430074, China*

Yunmin Liang − *School of Energy and Power Engineering, Huazhong University of Science and Technology, Wuhan 430074, China*

Rui Long − *School of Energy and Power Engineering, Huazhong University of Science and Technology, Wuhan 430074, China;* orcid.org/0000-0003-4911-1716

Wei Liu − *School of Energy and Power Engineering, Huazhong University of Science and Technology, Wuhan 430074, China*

Complete contact information is available at: https://pubs.acs.org/10.1021/acsami.1c03395

Author Contributions

‡Ji Li and Zikang Zhang have equal contribution to this work.

Funding

The study was supported by the National Natural Science Foundation of China (Nos. 51776079 & 52076088) and the Open Research Fund of Key Laboratory of Space Utilization, Chinese Academy of Sciences (No. LSU-KFJJ-2019-07).

Notes

The authors declare no competing financial interest.

■ ACKNOWLEDGMENTS

The authors thank the National Supercomputer Center in Tianjin for providing computing resources.

■ REFERENCES

(1) Gingerich, D. B.; Mauter, M. S. Quantity, Quality, and Availability of Waste Heat from United States Thermal Power Generation. *Environ. Sci. Technol.* **2015**, *49*, 8297−8306.

(2) Lu, H.; Price, L.; Zhang, Q. Capturing the invisible resource: Analysis of waste heat potential in Chinese industry. *Appl. Energy* **2016**, *161*, 497−511.

(3) Yu, B.; Duan, J.; Cong, H.; Xie, W.; Liu, R.; Zhuang, X.; Wang, H.; Qi, B.; Xu, M.; Wang, Z. L.; et al. Thermosensitive crystallization-boosted liquid thermocells for low-grade heat harvesting. *Science* **2020**, *370*, 342−346.

(4) Liu, Y.; Chen, Y.; Ming, J.; Chen, L.; Shu, C.; Qu, T.; Tan, Q.; Liu, Y.; Asefa, T. Harvesting waste heat energy by promoting H+-ion concentration difference with a fuel cell structure. *Nano Energy* **2019**, *57*, 101−107.

(5) Tocci, L.; Pal, T.; Pesmazoglou, I.; Franchetti, B. Small scale Organic Rankine Cycle (ORC): A techno-economic review. *Energies* **2017**, *10*, 1−26.

(6) He, J.; Tritt, T. M. Advances in thermoelectric materials research: Looking back and moving forward. *Science* **2017**, *357*, No. eaak9997.

(7) Barragán, V. M.; Kjelstrup, S. Thermo-osmosis in Membrane Systems: A Review. *J. Non-Equilib. Thermodyn.* **2017**, *42*, 217−236.

(8) Fu, L.; Merabia, S.; Joly, L. Understanding Fast and Robust Thermo-osmotic Flows through Carbon Nanotube Membranes: Thermodynamics Meets Hydrodynamics. *J. Phys. Chem. Lett.* **2018**, *9*, 2086−2092.

(9) Marbach, S.; Bocquet, L. Osmosis, from molecular insights to large-scale applications. *Chem. Soc. Rev.* **2019**, *48*, 3102−3144.

(10) Straub, A. P.; Yip, N. Y.; Lin, S.; Lee, J.; Elimelech, M. Harvesting low-grade heat energy using thermo-osmotic vapour transport through nanoporous membranes. *Nat. Energy* **2016**, *1*, 16090.

(11) Mahmoudi, F.; Date, A.; Akbarzadeh, A. Further investigation of simultaneous fresh water production and power generation concept by permeate gap membrane distillation system. *J. Membr. Sci.* **2019**, *572*, 230−245.

(12) Shaulsky, E.; Karanikola, V.; Straub, A. P.; Deshmukh, A.; Zucker, I.; Elimelech, M. Asymmetric membranes for membrane distillation and thermo-osmotic energy conversion. *Desalination* **2019**, *452*, 141−148.

(13) Straub, A. P.; Elimelech, M. Energy Efficiency and Performance Limiting Effects in Thermo-Osmotic Energy Conversion from Low-Grade Heat. *Environ. Sci. Technol.* **2017**, *51*, 12925−12937.

(14) Park, K.; Kim, D. Y.; Yang, D. R. Theoretical Analysis of Pressure Retarded Membrane Distillation (PRMD) Process for

Simultaneous Production of Water and Electricity. *Ind. Eng. Chem. Res.* **2017**, *56*, 14888−14901.
(15) Chen, X.; Boo, C.; Yip, N. Y. Low-temperature heat utilization with vapor pressure-driven osmosis: Impact of membrane properties on mass and heat transfer. *J. Membr. Sci.* **2019**, *588*, 117181.
(16) Bajraktari, N.; Hélix-Nielsen, C.; Madsen, H. T. Pressure retarded osmosis from hypersaline sources — A review. *Desalination* **2017**, *413*, 65−85.
(17) Yuan, Z.; Yu, Y.; Wei, L.; Sui, X.; She, Q.; Chen, Y. Pressure-retarded membrane distillation for simultaneous hypersaline brine desalination and low-grade heat harvesting. *J. Membr. Sci.* **2020**, *597*, 117765.
(18) Li, J.; Gao, S.; Long, R.; Liu, W.; Liu, Z. Self-pumped evaporation for ultra-fast water desalination and power generation. *Nano Energy* **2019**, *65*, 104059.
(19) Xu, Z.; Zhang, L.; Zhao, L.; Li, B.; Bhatia, B.; Wang, C.; Wilke, K. L.; Song, Y.; Labban, O.; Lienhard, J. H.; et al. Ultrahigh-efficiency desalination: Via a thermally-localized multistage solar still. *Energy Environ. Sci.* **2020**, *13*, 830−839.
(20) Zhang, Z.; Zhao, R.; Liu, Z.; Liu, W. Application of biporous wick in flat-plate loop heat pipe with long heat transfer distance. *Appl. Therm. Eng.* **2021**, *184*, 116283.
(21) Deshmukh, A.; Elimelech, M. Understanding the impact of membrane properties and transport phenomena on the energetic performance of membrane distillation desalination. *J. Membr. Sci.* **2017**, *539*, 458−474.
(22) Long, R.; Lai, X.; Liu, Z.; Liu, W. Direct contact membrane distillation system for waste heat recovery: Modelling and multi-objective optimization. *Energy* **2018**, *148*, 1060−1068.
(23) Lawson, K. W.; Lloyd, D. R. Membrane distillation. *J. Membr. Sci.* **1997**, *124*, 1−25.
(24) Deshmukh, A.; Boo, C.; Karanikola, V.; Lin, S.; Straub, A. P.; Tong, T.; Warsinger, D. M.; Elimelech, M. Membrane distillation at the water-energy nexus: Limits, opportunities, and challenges. *Energy Environ. Sci.* **2018**, *11*, 1177−1196.
(25) Yuan, Z.; Wei, L.; Afroze, J. D.; Goh, K.; Chen, Y.; Yu, Y.; She, Q.; Chen, Y. Pressure-Retarded Membrane Distillation for Low-Grade Heat Recovery: The Critical Roles of Pressure-Induced Membrane Deformation. *J. Membr. Sci.* **2019**, *579*, 90−101.
(26) Jian, S.; Zhu, J.; Jiang, S.; Chen, S.; Fang, H.; Song, Y.; Duan, G.; Zhang, Y.; Hou, H. Nanofibers with Diameter Below One Nanometer from Electrospinning. *RSC Adv.* **2018**, *8*, 4794−4802.
(27) Brown, T. D.; Dalton, P. D.; Hutmacher, D. W. Direct Writing by Way of Melt Electrospinning. *Adv. Mater.* **2011**, *23*, 5651−5657.
(28) Lu, Z.; Wilke, K. L.; Preston, D. J.; Kinefuchi, I.; Chang-Davidson, E.; Wang, E. N. An Ultrathin Nanoporous Membrane Evaporator. *Nano Lett.* **2017**, *17*, 6217−6220.
(29) Li, Y.; Alibakhshi, M. A.; Zhao, Y.; Duan, C. Exploring Ultimate Water Capillary Evaporation in Nanoscale Conduits. *Nano Lett.* **2017**, *17*, 4813−4819.
(30) Nazari, M.; Masoudi, A.; Jafari, P.; Irajizad, P.; Kashyap, V.; Ghasemi, H. Ultrahigh Evaporative Heat Fluxes in Nanoconfined Geometries. *Langmuir* **2019**, *35*, 78−85.
(31) Plimpton, S. Fast parallel algorithms for short-range molecular dynamics. *J. Comput. Phys.* **1995**, *117*, 1−42.
(32) Humphrey, W.; Dalke, A.; Schulten, K. VMD: Visual molecular dynamics. *J. Mol. Graphics* **1996**, *14*, 33−38.
(33) Jorgensen, W. L.; Chandrasekhar, J.; Madura, J. D.; Impey, R. W.; Klein, M. L. Comparison of simple potential functions for simulating liquid water. *J. Chem. Phys.* **1983**, *79*, 926.
(34) Jorgensen, W. L.; Maxwell, D. S.; Tirado-Rives, J. Development and testing of the OPLS all-atom force field on conformational energetics and properties of organic liquids. *J. Am. Chem. Soc.* **1996**, *118*, 11225−11236.
(35) Heinz, H.; Vaia, R. A.; Farmer, B. L.; Naik, R. R. Accurate simulation of surfaces and interfaces of face-centered cubic metals using 12−6 and 9−6 lennard-jones potentials. *J. Phys. Chem. C* **2008**, *112*, 17281−17290.
(36) Zhang, T.; Luo, T. Role of chain morphology and stiffness in thermal conductivity of amorphous polymers. *J. Phys. Chem. B* **2016**, *120*, 803−812.
(37) Li, J.; Long, R.; Zhang, B.; Yang, R.; Liu, W.; Liu, Z. Nano heat pump based on reverse thermo-osmosis effect. *J. Phys. Chem. Lett.* **2020**, *11*, 9856−9861.

https://doi.org/10.1021/acsami.1c03395
ACS Appl. Mater. Interfaces 2021, 13, 21371−21378